International Journal of Rock Mechanics & Mining Sciences 201 (2026) 106477

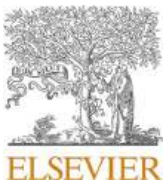

Contents lists available at ScienceDirect

International Journal of Rock Mechanics and Mining Sciences

journal homepage: www.elsevier.com/locate/ijrmms

Integrating 3D Point Cloud analysis for potentially unstable rock blocks characterization: a method for assessing size and shape distribution

G. Mineo [a], A. Riquelme [b], M. Rosone [c,*], C. Cappadonia [a]

[a] University of Palermo, Department of Earth and Marine Sciences, Palermo, Italy
[b] University of Alicante, Department of Civil Engineering, Alicante, Spain
[c] University of Palermo, Department of Engineering, Palermo, Italy

A B S T R A C T

This study presents a novel workflow for characterizing potentially unstable rock blocks using high-resolution 3D point clouds, addressing some of the limitations of traditional methods in rockfall risk analysis. The proposed methodology integrates block segmentation, 3D modelling using triangulation meshing algorithm, and the quantitative extraction of parameters such as volume, surface area, and shape. Moreover, a new parameter for block flattening, derived from the Oriented Minimum Bounding Box (OMBB), has been introduced and employed to conceptually update the existing shape classification system, enabling a more accurate representation of real block geometries. The workflow generates 3D Block Size Distribution and a refined Block Shape Classification, offering essential insights into fractured rock mass behavior and supporting geoengineering assessments and decision-making.

Validation through synthetic datasets of primitive three-dimensional shapes demonstrates the accuracy of the proposed method in calculating volumes and surfaces, as well as for improved shape classification. Application to a real case study on Mount Gallo (Sicily, Italy) shows good agreement between directly measured and indirectly calculated block volumes and reveals the dominant morphometric classes located on the rock slope.

Sensitivity analyses highlight the robustness of the volume calculation method to varying input data resolution and completeness, although large data gaps may affect accuracy. An uncertainty analysis, employing a non-parametric approach, ensures statistical reliability in defining the 95% confidence interval of the 3D Block Size Distribution. Overall, this proposed framework offers a robust and practical tool for rockfall risk management, providing detailed insights into individual potentially unstable blocks.

1. Introduction

The management of the rockfall risk remains a critical challenge for the safety of infrastructures and communities living near to rock slopes prone to instability. In this context, the knowledge of the characteristics of potentially unstable rock blocks is a fundamental step in risk assessment and in the implementation of effective mitigation measures. The size and shape of blocks within a rock mass are fundamental geomechanical parameters, certainly related to the complex interaction of discontinuities.[1]

Traditionally, the characterization of rock blocks is conducted through direct geomechanical surveys involving manual field measurements.[2] Even if these methodologies offer valuable data, they are still subject to limitations in terms of operator safety, accessibility, economic resources, required time and the ability to capture the geometric complexity of an entire rock mass.

In recent decades, the advent of high-resolution data acquisition technologies, such as terrestrial laser scanning [3–5] and photogrammetry [6–9] has revolutionized the approaches to rock masses studies and monitoring. These techniques allow the generation of dense and accurate 3D point clouds, providing a detailed representation of the rock surfaces and their discontinuities. The scientific community has rapidly moved towards the optimization of these data, developing open-source procedures for the characterization of discontinuities.[10,11] Moreover, the availability of high-resolution point clouds has opened new frontiers making possible the remote characterization of unstable blocks [12–14]. Obviously, data acquisition alone is not sufficient; a robust and rigorous methodology is needed to transform point clouds into a meaningful source of geomechanical information. This implies not only the identification of blocks, but also their accurate three-dimensional modelling and the extraction of quantitative parameters such as volume, surface, and shape, which are fundamental for a correct understanding of rock mass behavior, the rockfall risk analysis and for risk mitigation design.

In this regard, the volume information, together with the altmetric position of the block on the rock mass and its potential velocity during detachment and fall, represents a key element in assessing the magnitude of the rockfall phenomenon.

As suggested by Farmakis et al.,[15] it is crucial to distinguish between

* Corresponding author.
E-mail address: marco.rosone@unipa.it (M. Rosone).

https://doi.org/10.1016/j.ijrmms.2026.106477
Received 17 November 2025; Received in revised form 21 January 2026; Accepted 20 February 2026
Available online 27 February 2026

a rockfall event and a potentially unstable rock volume when applying rock masses characterization from point clouds. In contrast to the assessment of potentially unstable blocks, the analysis of rockfall volumes has been extensively investigated over the last decade, primarily through change detection approaches based on the comparison of multi-temporal models.

In this regard, Carrea et al.[16] and DiFrancesco et al.[17] critically highlighted the limitations of earlier automated extraction methods, demonstrating that rockfall inventories are highly sensitive to processing parameters. They showed that incorrect parameterization leads to significant errors: clustering of distinct events or artificial fragmentation, which directly distort both the volume estimates and the geometric shape of the detached blocks. Williams et al.[18] established that standard change detection suffers from event coalescence when the survey frequency is lower than the event frequency. This leads to an artificial inflation of block volumes and overestimation of the expected magnitude. Guerin et al.[19] demonstrated that volume detection thresholds are strictly method-dependent, ranging from millimeters for modern LiDAR to decimeters for historical Structure from Motion (SfM), with statistical censoring (rollover) occurring at even larger volumes for lower-resolution data.

The recent work by Farmakis et al.[15] represents a significant advancement in automated monitoring, introducing a non-parametric voxel-based approach to minimize user subjectivity in volumetric change detection. This effectively resolves the parameter sensitivity issues typical of earlier algorithms.

Watman et al.[20] demonstrated that kinematic feasibility is a strong predictor of block shape and size, suggesting that while the structural network defines the potential block volume, the final inventory is often finer, likely due to fragmentation processes not captured by the simulated model. According to the literature, three main traditional approaches are commonly used to estimate the volume of potentially unstable blocks: equation-based, statistical and direct measurements approaches.

The equation-based approach is easily applicable following a geomechanical survey. The geomechanical parameters that play a role include the orientation, spacing and persistence of the main discontinuity sets. One of the most applied is Palmstrom,[21] who related the spacing referred to the main discontinuity sets (S_1, S_2, S_3) with the sines of the angles (γ_{12}, γ_{23}, γ_{13}) formed between the sets themselves:

$$V_b = \frac{s_1 \cdot s_2 \cdot s_3}{\sin\gamma_{12} \cdot \sin\gamma_{23} \cdot \sin\gamma_{13}} \quad (1)$$

To overcome the main problem affecting deterministic approaches focused on obtaining a single characteristic volume which should represent the entire rock mass, the concept of In Situ Block Size Distribution (IBSD) as statistical approach took place.[22,23] The main purpose of this approach is to determine a cumulative distribution of volumes that could be generated by the intersections between the discontinuity sets[24] to better characterize a complex system like a rock mass. The approach to constructing the IBSD consists of ordering the population of volumetric values in ascending order to generate a cumulative curve, which represents the number of observations (frequency on the y-axis) that are less than or equal to a given volume (x-axis). According to Umili et al.,[24] equation (1) can be applied by statistically varying the spacing values, thereby producing a dataset of block volumes.

Moreover, as suggested by the same authors, the spacing values obtained from the geomechanical survey can be used to derive volume distributions using the Mount Carlo method: for each simulated combination of three discontinuities, the volume is calculated. This procedure is referred to as the Mount Carlo Cumulative Distribution Function (MCDF). Finally, the most used approach in rock slope engineering is the direct measurement of the unstable block's dimensions carried out by expert rock climbers. This approach presents several critical issues, including the technical difficulty involved in analyzing the whole rock mass and the hazardous conditions to which the operators are exposed.

Shape, as well as size, is a direct result of interactions among differently oriented discontinuities. As highlighted by Caviezel et al.,[25] a proper understanding of the block shape directly is essential for the development of more realistic rockfall propagation simulations. In fact, since the shape significantly influences the block-slope interaction during impacts, the probability of the block deviating its trajectory from a linear course is increased.

Regarding shape analysis, the main approach applied is based on morphometric indices[26–29]. However, these approaches provide information on the average dimensions of blocks but not details on the shape and size of individual blocks, which are often irregular due to the variability in the orientation of joints.

Wang et al.[29] developed a 3D shape index to describe the shape of individual quarry blocks. Smith[30] proposed a methodology based on stereographic techniques to determine block shape and size, interpreting dihedral angles and spacing between discontinuities.

Among the various methodologies, the Block Shape Characterization Method (BSCM) proposed by Kalenchuk et al.[31] has found wide application for the characterization of block shape and shape distribution in rock masses, particularly when using data obtained from numerical methods. This method classifies blocks into six well-defined categories: cubic, cubit-to-elongated, elongated, elongated-to-platy, platy, platy-to-cubic. The BSCM uses two dimensionless parameters, α and β, which are plotted in a triangular diagram. Parameter α describes the block surface-to-volume ratio, while parameter β quantifies the average angle between vectors defined by the major inter-vertex dimensions (chord length values above the median), including all edges, face diagonals, and internal diagonals. The diagram area is divided into sectors to which a specific shape is associated. The main limitation of this approach lies in the need to know the coordinates of every vertex of all blocks in the considered rock mass, a relatively simple task when applying Discrete Fracture Network (DFN) models since the system was designed for these applications. Despite this limitation, the BSCM is widely used in literature [32–36] for its simplicity and its ability to provide detailed characterization.

The main objective of the present work is to develop a workflow that allows the derivation of quantitative information, such as the dimensional distribution (3D Block Size Distribution) and morphometric classification (Block Shape Classification) of potentially unstable rock blocks via 3D point cloud data. The following sections will be focused on the phases of the process, starting from the segmentation of blocks on the point cloud using open-source software. The meshing algorithm, which enables the generation of watertight and manifold 3D models and ensures the accuracy of volume and surface calculations, will also be presented. Subsequently, the most effective statistical techniques for processing the acquired volumetric dataset and extracting key statistical parameters will be explored.

Moreover, a new dimensional parameter based on the Oriented Minimum Bounding Box (OMBB), has been introduced and used to conceptually update the existing shape classification system, making it applicable also to complex, real shapes. All these computational steps have already been implemented in ad hoc Python code, which allows automated processing of point cloud data and the definition of volumetric and geometric parameters.

To validate the effectiveness of the proposed method, two case studies were presented: a synthetic dataset of three-dimensional primitive shapes and a dataset of real rock blocks acquired from a portion of the rock slope of Mount Gallo (Sicily, Italy). Sensitivity analyses were conducted to evaluate the impact of input data quality on the results, and an uncertainty analysis was carried out to quantify the reliability of the acquired statistics. The integration of these analyses aims to provide a comprehensive and robust framework for the characterization of potentially unstable rock blocks, which can be regarded as a step toward the development of a digital twin for modern geomechanics and risk management.

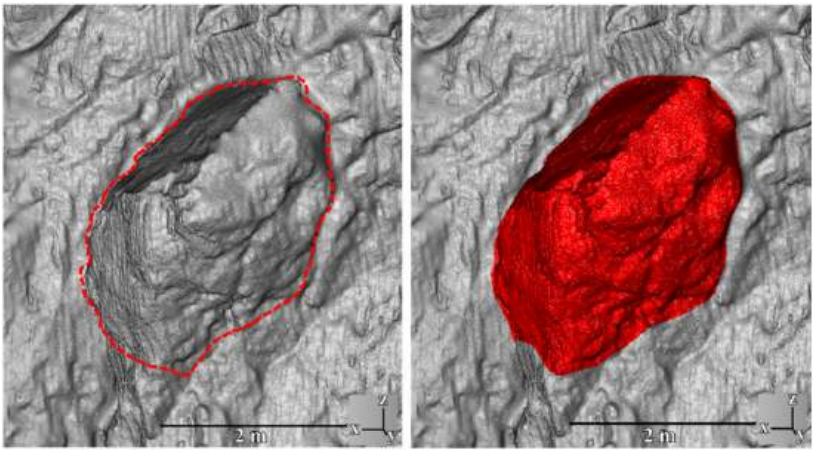

Fig. 1. Example of segmentation for a potentially unstable block identified on the rock slope.

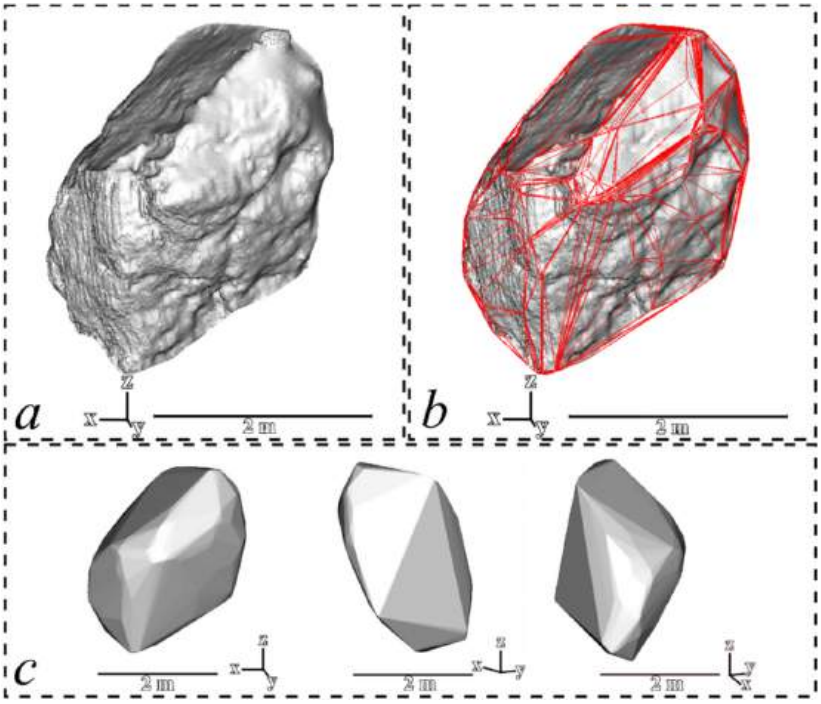

Fig. 2. a) Point cloud representing a potentially unstable block; b) Application of the Convex Hull algorithm; c) different visualization of the modelled block.

2. Methodology

2.1. Segmentation procedure and meshing algorithm

The characterization of potentially unstable blocks starting from high-resolution point clouds begins with their recognition on the modelled rock mass.

In particular, the segmentation of potentially unstable blocks is conducted on the point cloud within the open-source software CloudCompare (2.13.2) using the segmentation tool (Fig. 1) by applying an expert-guided approach.[12,14] The result of the segmentation process is a dataset of convex point clouds representing the recognized blocks. A fundamental step to ensure the reliability of the segmented point cloud, representing a potentially unstable block is the a priori filtering process. For point clouds derived from TLS, the intensity (which is a parameter related to how reflective an object is at the specific wavelength of the laser) registered for each point can be used to discriminate between rock and noise. In supplementary material, note A an example of size and shape analysis for a block affected by noise is presented.

The next step is to define a continuous and closed 3D model that, when applied to each block, allows obtaining information useful for its characterization, such as volumes and surfaces. For this purpose, a triangulation meshing algorithm was implemented in a Python environment resulting in a mesh that is watertight and manifold, meaning it is free of holes and every edge of the mesh is shared by only two faces and there are no complex intersecting geometries.[37]

This type of meshing is based exclusively on the position of points in three dimensions, exploiting geometric criteria such as Delaunay triangulation. Such algorithms, since they natively allow obtaining watertight meshes enveloping the true shape, even from open point clouds, are defined as “Convex Hull”. The behavior of the algorithm at the edges of the convex surface will follow the Delaunay criterion, closing the point cloud through wider triangles. The external faces of these wider triangles will represent the surface on which the block may slide; this concept has already been applied[14] for the definition of the volumes of potentially unstable blocks by exploiting tools available on

CloudCompare software. The result of the triangulation is a 3D model represented by a list of vertices that form the hull and a list of faces that compose the external surface of the polyhedron. Once the representation of the convex polyhedron is completed, it is possible to calculate its volume and surface through decomposition into adjacent tetrahedra. Fig. 2 displays an application of convex hull algorithm to the block previously segmented from the point cloud in Fig. 1.

2.2. 3D Block Size Distribution

The previous steps, when applied to a rock mass, typically result in a dataset of volumes that can be statistically treated. The 3D Block Size Distribution emerges as a robust tool for describing the dimensional variability of the potentially unstable blocks recognized and processed from 3D point clouds. Analysis of this distribution allows the definition of descriptive statistics such as symmetry/asymmetry and multimodality as well as the definition of quantitative parameters that can support engineering design for risk mitigation (e.g. rockfall barriers).

The 3D Block Size Distribution, adapted from the In Situ Block Size Distribution,[38] represents the probability that a block has a volume less than or equal to a given value, providing an immediate overview of the proportion of blocks that fall into a specific dimensional class.

From the cumulative curve, it is possible to extract the following crucial quantitative statistical parameters: Median (50th percentile), which indicates the volume below which 50% of the blocks fall, providing a robust measure of the central size of the population; other quartiles (25th and 75th percentile) delineating the lower 25% and upper 25% of the distribution, respectively, offering an indication of data dispersion around the median; upper percentiles (e.g., 90th, 95th, 99th percentile), which are particularly relevant in engineering design, as they allow identifying the dimensions of the largest falling blocks present in the system. In particular, the 95th percentile (p95) is a widely used statistic in various scientific fields and is being adopted as a standard (e.g. ONR 24810,[39] 2017; UNI 11211-3:2018, 2018[40]) for the design of risk mitigation works. It represents the volume below which 95% of the blocks are found, implying that only 5% of the blocks have a volume greater than this value.

2.3. Block shape classification

Volume and surface information are not enough to define the characteristics of a block; for a more useful characterization, the introduction of morphometric indicators representative of the block morphology is essential.

To introduce these parameters, the classification adopted in the workflow was conceptually derived by the Kalenchuk et al.[31] shape classification system, which was subsequently updated to better represent real block geometry. As previously mentioned in the paper, it relies on easily accessible data from DFN models. Actually, such parameters are also easily available for blocks modelled according to convex hull algorithms, whereas they are not straightforward to derive when traditional methods are applied. This explains why, to date, no applications of the Block Shape Characterization Method have been carried out on real-shape blocks.

In the classification system, α relates surface area (A_s), Volume (V), and the average chord length between all vertices (L_{avg}) according to the following:

$$\alpha = \frac{A_s \cdot L_{avg}}{7.7 \cdot V} \tag{2}$$

In the formula, the value 7.7 is a correction factor to make α equal to 1 for a cube.

For β, the median among all chord lengths is defined, and values below the median are excluded from the calculation. Thus, β is related to the square of the ratio between the sums of the scalar products between chords a and b greater than or equal to the median and the products of the moduli of the vectors for the same a and b:

$$\beta = 10\left[\frac{\sum (a \cdot b)^2}{\sum \|a\|^2 \cdot \|b\|^2}\right]^2 \tag{3}$$

In this relationship, the value 10 is used as a scale factor. Both α and β are defined on the interval $[0, +\infty)$. In particular, the authors defined the range [1, 10] in the classification diagram as the most useful for classifying the shapes of the modelled blocks.

In β, the reason for using chords greater than or equal to the median is expressed by the authors themselves and refers to the greater influence that longer chords have in defining the degree of elongation of the shape to be classified. Therefore, by analyzing all the longer chords, an accurate evaluation of the degree of elongation of the shape is obtained.

For α, the key assumption is that the degree of flattening is primarily controlled by the area-to-volume ratio including in the denominator the correction factor 7.7 that normalizes the value to 1 for the cubic form. In the present study, the authors suggest that while the assumption may hold true, it is not entirely unambiguous. To ensure that α defines the degree of block flattening more effectively, a modification to the calculation method was proposed, introducing a correction factor defined on the main dimensions of the Oriented Minimum Bounding Box (OMBB), i.e., the smallest box that inscribes the block and orients itself with respect to it. Once the OMBB is constructed around the 3D block, its dimensions can be known to evaluate its shape. In particular, the ratio between the width (w) and the thickness (t) represents the flattening index of the box:

$$F = \frac{w}{t} \tag{4}$$

Since, by its characteristics, the OMBB has dimensions approximately equal to the maximum dimensions of the inscribed block, it is possible to assume that F index$_{OMBB} \approx F$ index max$_{block}$. This index can, therefore, be used as a Flattening correction factor (F) for the calculation of α_F (α Flattening) as follows:

$$\alpha_F = \frac{A_s \cdot L_{avg}}{7.7 \cdot F^{-1} \cdot V} \tag{5}$$

Note that when w is equal to t, then F is equal to 1, and α_F (α Flattening) will be equal to standard α, maintaining the considerations made by Kalenchuk et al., regarding the normalization of the classification system with respect to the cube.

The procedure for analyzing the size and shape of identified potentially unstable blocks was implemented in a Python environment, from which the Advanced BLOck MOrphometry and Volume analyser (ABLOMOV) was created and made available as a Graphical User Interface (see supplementary material, note B).

2.4. Sensitivity analysis

To evaluate the impact that the quality of input data has on the application of the proposed method for volume calculation, a sensitivity analysis was conducted using two different approaches. The first test aims to evaluate the impact of data resolution, while the second enables the assessment of the effect of completeness.

The test on the influence of resolution for volume calculation was first conducted on three primitive shapes built in CloudCompare: a cube with a 1-m side, a sphere with a 2-m radius, and a cylinder with a 2-m radius and a 5-m height. The obtained meshes were sampled to create point clouds with variable resolution: 0.5 cm, 1 cm, and 2 cm. Following this, the same approach was employed for a real block.

Adopting the same methodology, to assess how the completeness of the input data affects the results, both a cube with a side length of 1 m built in CloudCompare and a real block were used as models. The cube with a volume of 1 m^3 and an area of 6 m^2 was modified to simulate

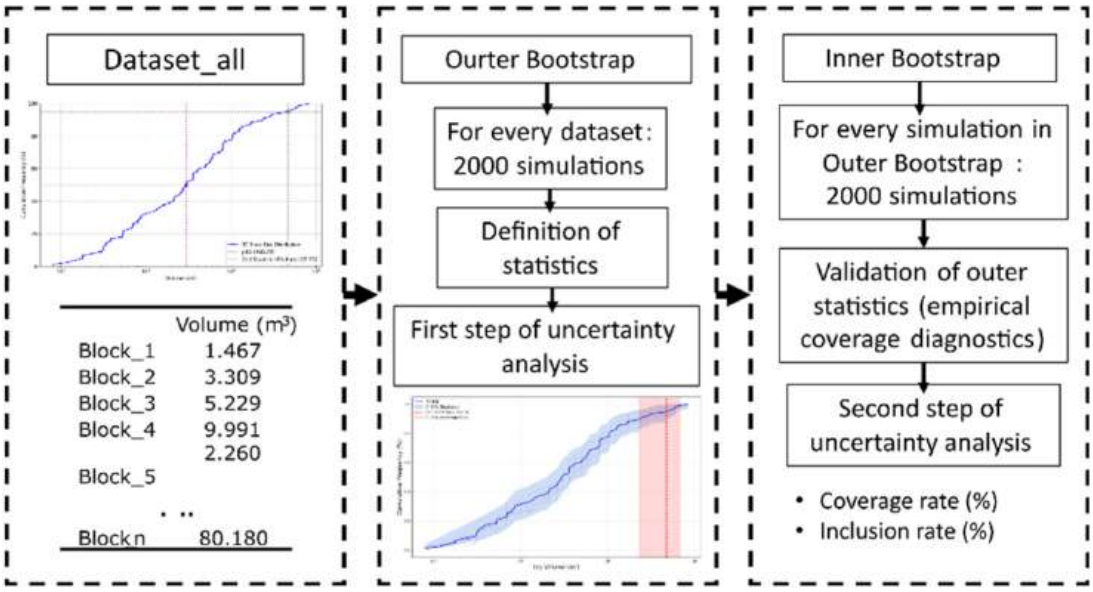

Fig. 3. Workflow for uncertainty analysis according to non-parametric statistical approach based on nested Bootstrap BCA.

possible real scenarios:

a) A block whose all faces are known except the inner one
b) A wedge block whose two intersecting faces and the intersection line on which sliding would occur are not known
c) A block embedded between blocks on two sides
d) A wedge block of which only two faces are exposed on the rock front.

2.5. Uncertainty analysis

As already analyzed in previous sections, from the simple reordering of data, it is possible to construct a cumulative curve that represents useful information for characterizing volumes in a rock mass. Following the selection of the appropriate statistics for rockfall barrier design purposes, a crucial step is evaluating the uncertainty in defining these values.

The statistical treatment of the dataset can be carried out using parametric and non-parametric statistical approaches. The former approximates the dataset to a known distribution, as determinate by goodness-of-fit tests [41–43]. Based on other authors results,[44,45] who analyzed uncertainty on variable size volumetric datasets obtained with Monte Carlo simulations, emerges that the larger the sample size, the greater the reliability of the tests applied for defining the distribution that best approximates the dataset. This condition is even more critical if one considers the high dispersion that typically characterizes a dataset of natural values.

The datasets resulting from the proposed method for recognizing and calculating the volumes of blocks are small and present a high range of values (about 3 orders of magnitude difference between the minimum and maximum value), so a non-parametric approach was proposed to perform the uncertainty analysis. In particular, a workflow applying a robust statistical approach based on Bias-Corrected and Accelerated (BCA[46]) Bootstrap was chosen to construct and validate the 95% confidence interval of the 3D Block Size Distribution (Fig. 3).

Bootstrapping is a powerful and versatile statistical resampling technique that enables the estimation of the distribution for statistics when a single data sample is processed. The basic principle of bootstrapping is to repeatedly extract many equally sized "bootstrap samples" randomly resampling with replacement with respect to the original dataset (e.g., 1000–10,000 times). The latter is a crucial point of the method because each data point in the original set has the same probability of being selected for a bootstrap sample and can appear more than once in the same sample. This procedure allows capturing sampling variability and estimates standard errors and confidence intervals without making assumptions about the shape of the population distribution. Each bootstrap sample represents a possible sample that could have been obtained from the population. The BCA is an advanced variant of the bootstrap method that corrects for both bias and skewness in the simulated sampling distribution, thus yielding more accurate results.[46] This technique is particularly useful for natural data that often has highly skewed and noisy distributions [47–50].

As summarized in the workflow in Fig. 3, the bootstrap method was applied following a nested approach: starting from the complete dataset (dataset_all), 2000 simulations were performed (Outer Bootstrap), which allowed defining a first level of in-depth uncertainty analysis. Specifically, the 95% confidence interval was constructed around the 3D Block Size Distribution (3D-BSD), which allows determining, with 95% certainty, that the statistic of interest falls within the determined range. The next step (Inner Bootstrap) was useful in determining another 2000 simulations for each curve simulated in Outer Bootstrap. The purpose of this further level of analysis is to determine, on 2000 × 2000 datasets of greater variability, the reliability of the chosen confidence interval (CI 95%) and the statistics defined on the 3D-BSD. This is done by calculating two parameters: the coverage rate and the inclusion rate. The former evaluates how many times the 95th percentile (example of selected statistic from the 3D-BSD) calculated for each curve in Inner Bootstrap falls within the 95% CI calculated on Outer Bootstrap. The latter calculates how many times the real 95th percentile falls within the 95% CIs calculated on the Inner Bootstrap.

The coverage rate aims to estimate the accuracy of the chosen confidence interval, according to the principle that if the reference CI of BCA is a good estimator of the true population confidence interval, it can be expected to capture the 95th percentile of new samples (simulations from the same population) approximately 95% of the time. The inclusion rate, on the other hand, serves as an indicator of the representativeness of the sample dataset and, therefore, of its inferential repeatability. Specifically, if the starting dataset is an accurate representation of the population, a high inclusion rate suggests that the BCA confidence intervals, derived from new sample extractions (simulating new real data), are effective in containing the value of the statistic (the 95th percentile, in this case) observed in the original dataset.

In practical terms, a coverage rate close to 95% would indicate that the chosen confidence interval accurately estimates the uncertainty at 95%. A coverage rate lower or higher than 95% will indicate,

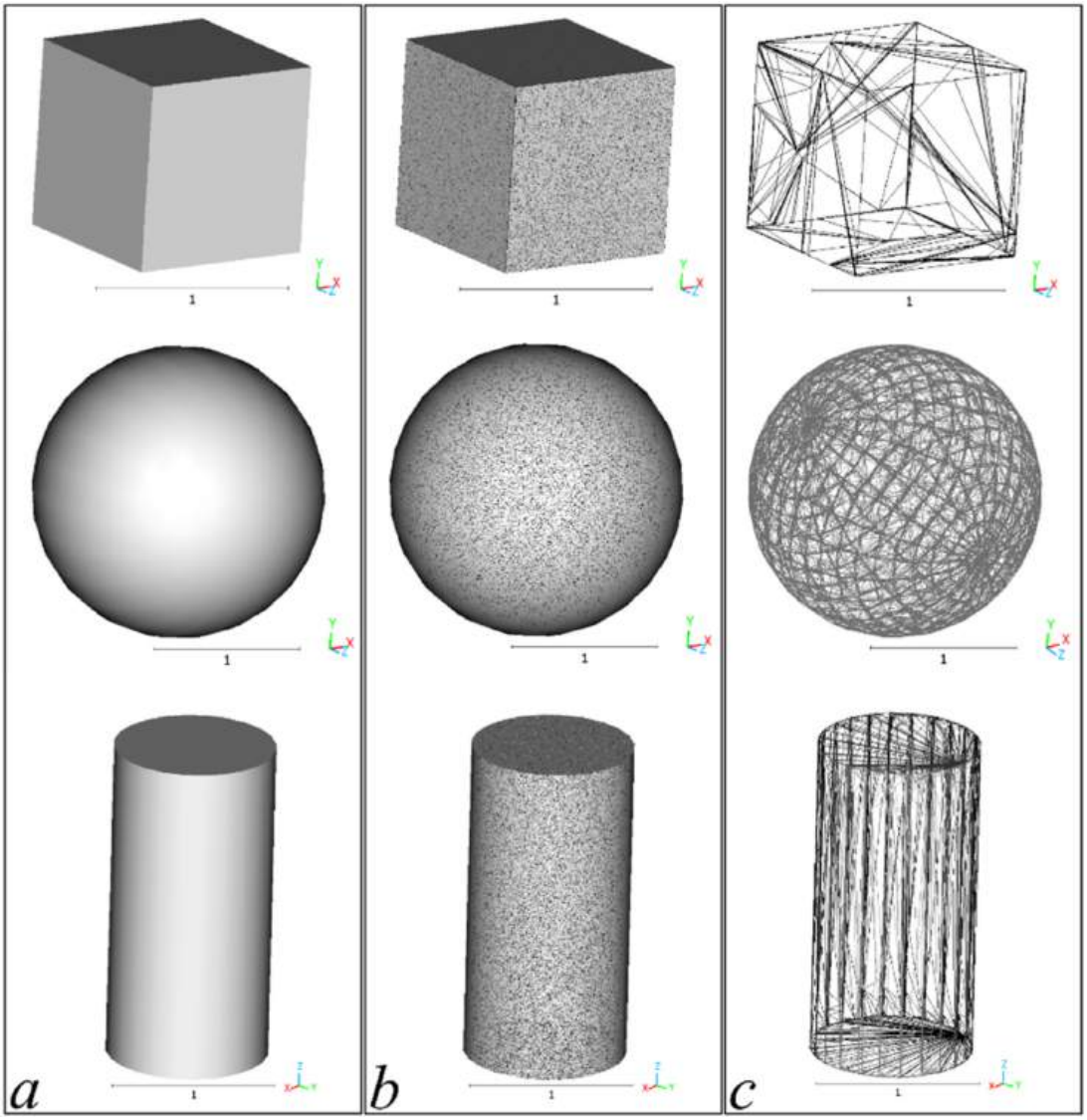

Fig. 4. Primitive three-dimensional shapes meshing. a) mesh created on CloudCompare (CC) for a cube, sphere and a cylinder; b) point clouds sampled from meshes; c) mesh resulting from Convex Hull (CH) algorithm for cube, sphere and a cylinder.

respectively, an underestimation or overestimation of the chosen confidence interval. The inclusion rate does not have an intuitive threshold value, but a high rate indicates consistency and stability because the higher it is, the more the original result can be considered capturable by similar intervals.

3. Case studies

To validate the effectiveness of the proposed method, two different applications are provided below. The first application concerns the processing of a synthetic dataset of primitive shapes, while the second application is carried out on a dataset of real rock blocks acquired on a portion of Mount Gallo, Sicily (Italy), affected by several rockfall phenomena.

3.1. Case study 1: primitive three-dimensional shapes

The case study was conducted using a synthetic dataset of primitive three-dimensional shapes built via CloudCompare (v. 2.13.2) software. Specifically, a cube of 1-m side, a sphere of 1-m radius, and a cylinder of 0.5-m radius and 2-m height were constructed by means of 3D meshed volumes (Fig. 4). For each shape whose real volume (V_{cc}) and surface area (S_{cc}) are known:

1. 3D point sampling was conducted on the meshed shapes to obtain 3D point clouds with a resolution of 1 cm;
2. The Convex Hull algorithm was applied to the 3D point clouds to build new meshes and recalculate volume (V_{CH}) and surface area (S_{CH}) on them;
3. The calculation of α and β was applied to the meshes resulting from the Convex Hull for both the original and β-α_F shape classification systems.

3.2. Case study 2: dataset of blocks on a rock slope

The central-northern sector of the Sicilian coast is characterized by isolated carbonate reliefs alternating with intensively inhabited coastal plains. Mount Gallo (Fig. 5) is affected by high-angle discontinuity systems with high frequency, which, by intersecting with the sub-horizontal stratification system, define a block configuration. The sector is strongly affected by rockfall phenomena. In particular, the southern slope overlooks a densely urbanized area, while the northern

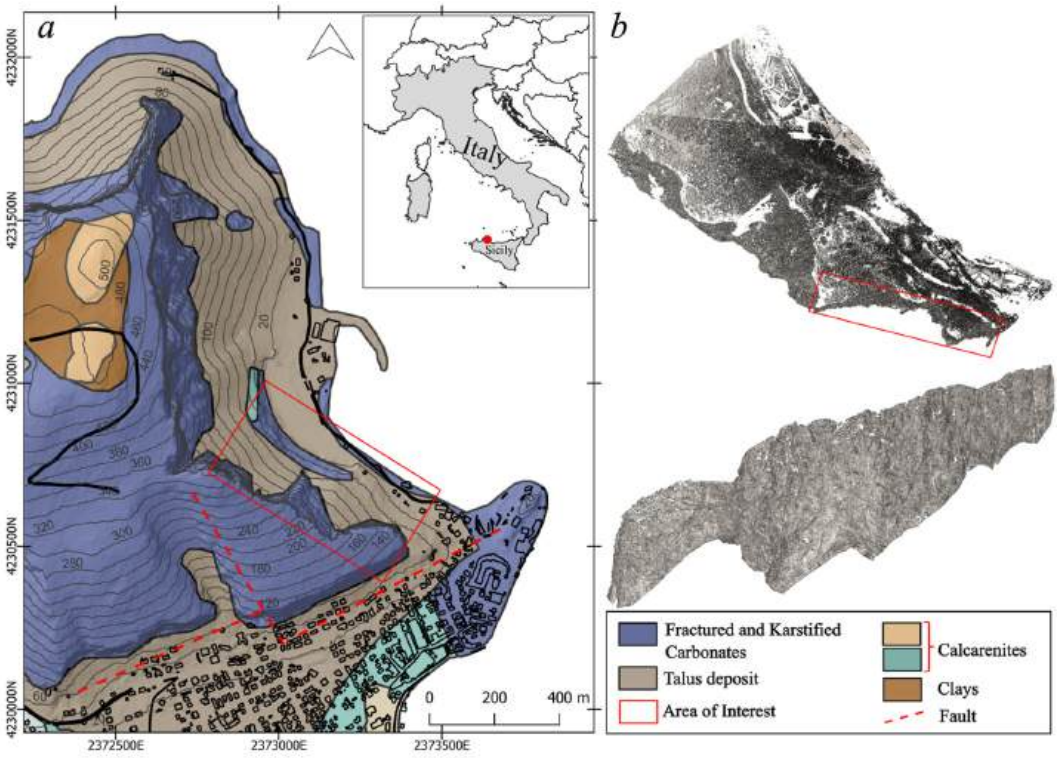

Fig. 5. Overview of the study area. a) geological settings of the area; b) point cloud acquired for the study area with focus on the rock slope.

and western slopes are steep cliffs facing a zone of remarkable touristic and natural interest. Consequently, the study area is characterized by high hazard and risk scenarios.

The Mount Gallo area has already been studied in the past using traditional approaches to assess rockfall hazard.[51] Recently, acquisitions conducted directly on the rock mass by expert rock climbers allowed determining the volume of some potentially unstable blocks based on the main dimensions measured. Manual surveys were carried out with the highest possible quality considering the acquisition conditions. Moreover, the chosen blocks were specifically selected for their accessibility and clearly defined boundaries, minimizing subjective interpretation. The subsequent remote survey campaign with a terrestrial laser scanner provided a high-resolution point cloud, within which the same blocks were identified. Therefore, for 11 blocks, a comparison was carried out between volumes obtained from direct measurements and those estimated using the proposed indirect methodology (Fig. 6).

4. Results

4.1. Size and shape estimation

Tests were performed to assess whether the α value, as currently applied, accurately represents the degree of flattening for both simple and real blocks. If one were to compare the values of α and β for a parallelepiped (P1) 1 m-length, width and thickness of 0.2 m with a parallelepiped (P2) 1 m-length, 1 m-width and 0.2 m-thickness, there would be an evident differentiation for the degree of elongation ($\beta_{P1} > \beta_{P2}$) while no substantial differences with respect to the degree of flattening ($\alpha_{P1} \sim \alpha_{P2}$) will be highlighted, despite the evidence of a flattening that characterizes P2 more than P1 (see Table 1). Fig. 7 show the results for blocks P1 and P2 plotted on the original triangular diagram by Kalenchuk et al. where the three fundamental shapes (Cubic, C; Elongated, E; Platy, P) and the three intermediate shapes (Cubic-Elongated, CE; Elongated-Platy, EP; Platy-Cubic, PC) are identified in six different regions based on the respective α and β values.

Table 2 details the parameters used to classify two real blocks, B1 and B2. Fig. 8 shows the actual shape of block B1 and block B2, together with their position on the triangular diagram, where the classification for the real blocks is reported using both the pairs (α, β) and (α_F, β). The resulting α values are 1.241 for block B1 and 1.164 for block B2. For the same blocks, the corresponding α_F values are 3.655 and 3.941, respectively. Specifically, according to the proposed modification, block B1 shifts from Cubic–Elongated (CE) to Elongated–Platy (EP), while block B2 changes from Cubic (C) to Platy–Cubic (PC). These new classifications clearly provide a more accurate representation of the actual shapes of the blocks.

The results obtained for case study 1 show an excellent overlap in the calculation of volume and surface from Convex Hull compared to the values obtained from CloudCompare (Table 3).

Regarding the parameters for shape classification, the differences between α and α_F are null for the cube. These considerations are also valid for the sphere, which has an $\alpha = \alpha_F$ of 0.520, and for the cylinder, which has an $\alpha = \alpha_F$ of 0.836. These results are consistent with those of the original shape classification system for simple non-flattened 3D geometries.

Differently, for the case of block P2 represented in Table 1, despite being a primitive shape, α value conveys the classification onto an equidimensional block (cubic class), while α_F highlights the flattened component (platy class).

Fig. 9 highlight the results obtained for case study 2 in which points represent the directly measured volumes (x-axis) and indirectly measured volumes (y-axis) for the 11 blocks analyzed. The calculated RMSE value of the datasets with respect to the diagonal (i.e. the condition in which the two datasets fit perfectly with each other) is 0.320.

Following the validation of the volume calculation method for potentially unstable blocks, the analysis was extended to the entire point cloud acquired for the rock slope. A total of 77 blocks were identified and segmented, and their volumes, calculated according to the proposed method, are represented in Fig. 10 in the form of a 3D Block Size Distribution.

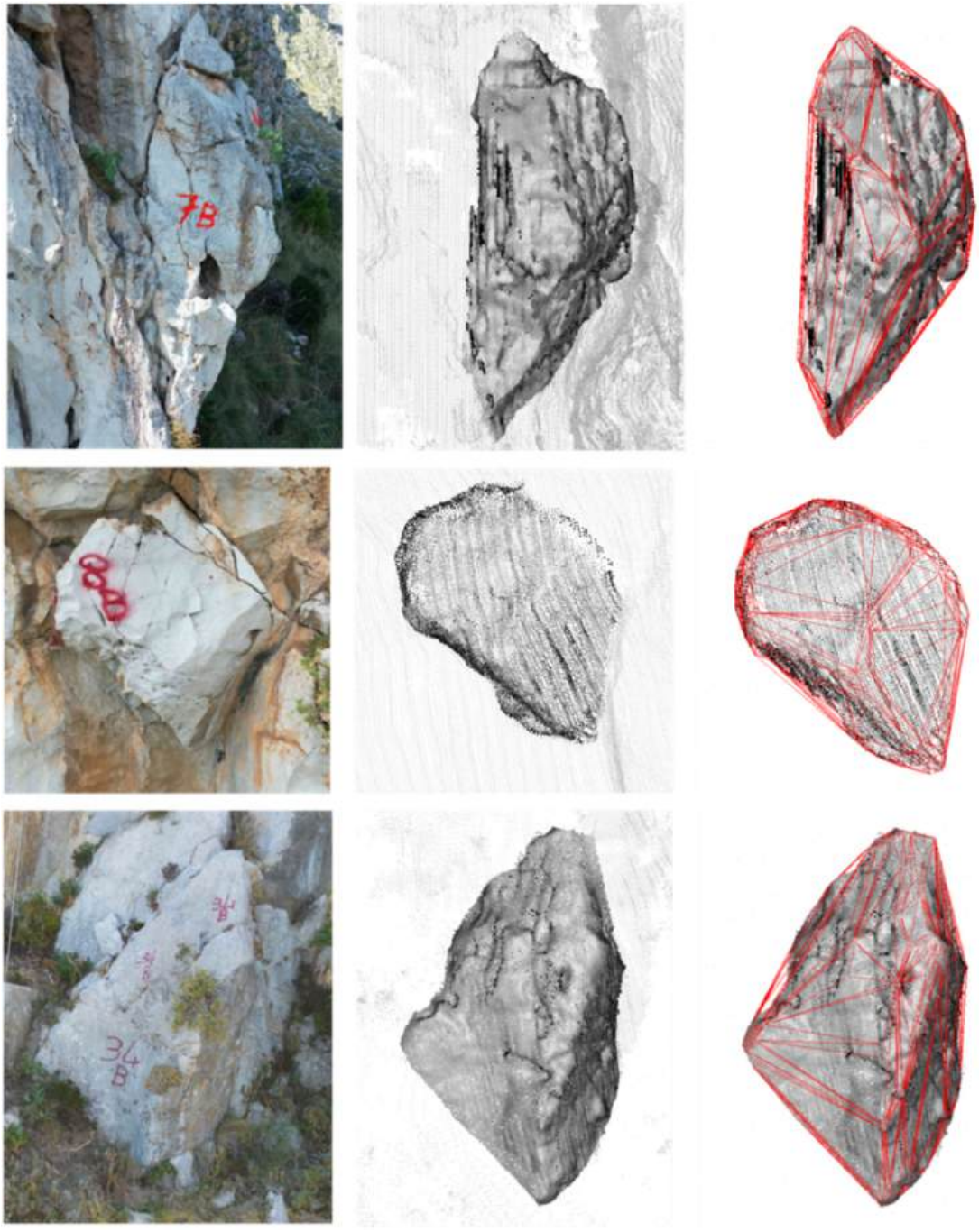

Fig. 6. Comparison between direct measurements and the proposed method for volume estimation for three out of eleven potentially unstable blocks. Convex Hull models resulting from ABLOMOV tool.

Table 1
Calculation of α, α_F and β values for P1 and P2 blocks according to the original and modified Block Shape Characterization Method by Kalenchuk et al., 2006.

	Dimensions (m)	Surface (m2)	Volume (m3)	Lavg (m)	F	α	α_F	β
P1	1 × 0.2 × 0.2	0.88	0.04	0.680	1	1.944	1.944	8.470
P2	1 × 1 × 0.2	2.8	0.2	1.012	5	1.840	9.2	1.959

The descriptive statistics in evidence are the median equal to 29.73 m^3, the 95th percentile (p95) equal to 468.70 m^3.

For each block, both BSCM and the α_F-β shape classification parameters were calculated according to the proposed methodology. The results were plotted on the triangular diagram for shape classification (Fig. 11). From the dispersion of the values, most of the blocks fall into the cubic class (52%). The second most represented class is cubic to elongate (29%). The cubic to platy, elongated, and platy to elongated classes follow with 13%, 5%, and 1% respectively.

The integrated analysis of volumes and shapes can provide

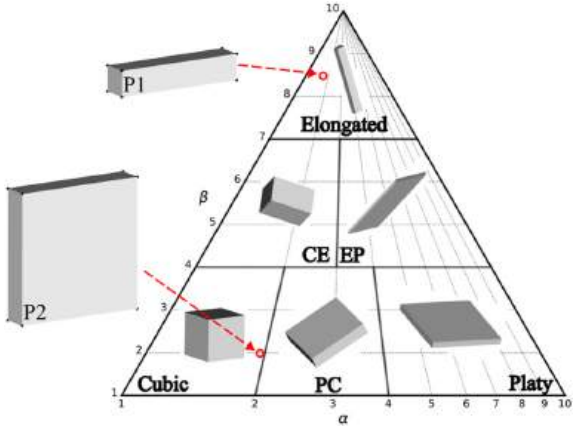

Fig. 7. Example of classification for two primitive shapes (P1 and P2) positioned on the triangular diagram from Kalenchuk et al., 2006 using the original BSCM system. CE (Cubic-Elongated), EP (Elongated-Platy), and PC (Platy-Cubic) are the intermediate shapes between Cubic (C), Elongated (E), and Platy (P). Modified from ABLOMOV results.

Table 2
Summary of the data necessary for the calculation of α_F and β for B1 and B2.

	Surface (m2)	Volume (m3)	L_{avg}(m)	F	α	α_F	β
B1	637.69	823.88	12.342	2.945	1.241	3.655	5.435
B2	35.77	11.11	2.784	3.386	1.164	3.941	3.133

information that would not be highlighted by traditional approaches only. In fact, blocks with larger volumes could have a shape that deviates from that of the most represented volumes delimited by the intersection of the main recognized discontinuity sets.

To obtain this level of detail, the volume information from the 3D Block Size Distribution, combined with the shape information obtained from the classification was plotted in the diagram in Fig. 12. The volumes were divided into five classes by choosing percentile ranges to have higher resolution on the higher values. Specifically, the class of blocks considered are: D < 50%, D50-75%, D75-90%, D90-95%, D > 95%.

What is observed is the predominance of volumes belonging to class D < 50% distributed with different frequencies across all morphometric classes in which the modelled blocks fall, except platy-to-elongated class. The graph in Fig. 13 shows that the CE class presents approximately 45% of the smaller-sized blocks, followed by the Cubic class with

Table 3
Size and shape results for case study 1. Volume and Surface area from CloudCompare (Vcc, Scc), Volume and Surface area from Convex Hull (Vch, Sch), α and β from Kalenchuck, α_F from this work approach.

	V_{CC}	V_{CH}	S_{CC}	S_{CH}	α	α_F	β
Cube	1 m^3	1 m^3	6 m^2	6 m^2	1	1	0.824
Sphere	4.123 m^3	4.123 m^3	12.468 m^2	12.468 m^2	0.520	0.520	1.364
Cylinder	1.552 m^3	1.553 m^3	7.818 m^2	7.817 m^2	0.836	0.836	5.447

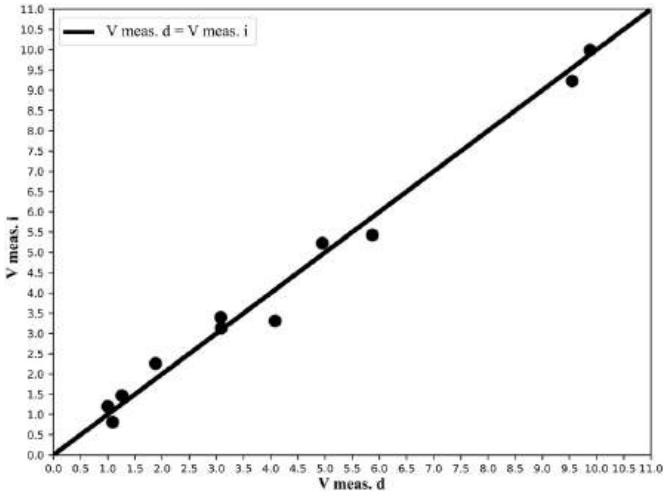

Fig. 9. Comparison between direct measurements and the proposed method for volume estimation of 11 blocks. Graphical representation of calculated volumes.

38% and by PC and Elongated with 11% and 6% respectively. The volumetric class D50-75% is distributed for 45% in the cubic morphometric class, while for 26% it falls into the CE class, for 23% into the PC class, and for 5% into the Elongated class. The volumetric class D75-90% falls into the Cubic class for 86%, PC for 7%, and CE for 7%. The volumetric class D90-95% falls into the Cubic class for 22%, PC for 51%, and CE for 27%. Finally, the D > 95 class falls for 44% in Cubic, for 33% in EP, and for 23% in Elongated.

4.2. Sensitivity analysis

The sensitivity analysis performed on primitive shapes was based on resolutions chosen as typically obtained by LiDAR acquisitions and

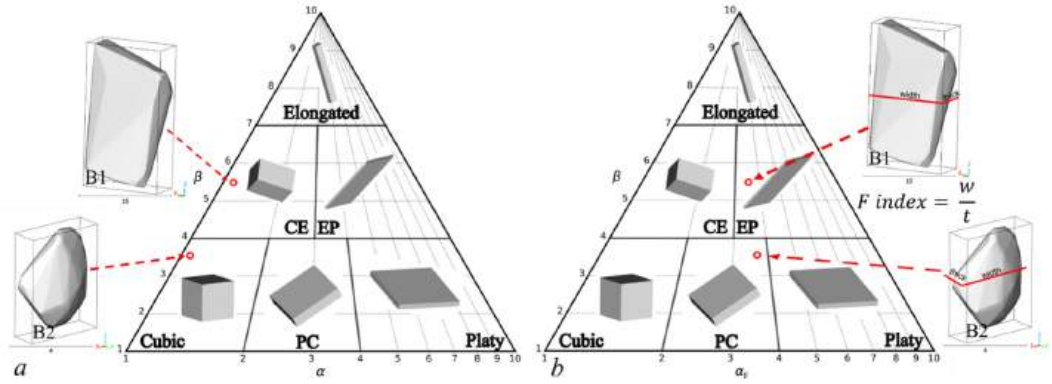

Fig. 8. a) Classification of B1 and B2 blocks according to Kalenchuck et al., 2006; b) Classification of the same blocks applying β-α_F shape classification. CE (Cubic-Elongated), EP (Elongated-Platy), and PC (Platy-Cubic) are the intermediate shapes between Cubic (C), Elongated (E), and Platy (P). Modified from ABLOMOV results.

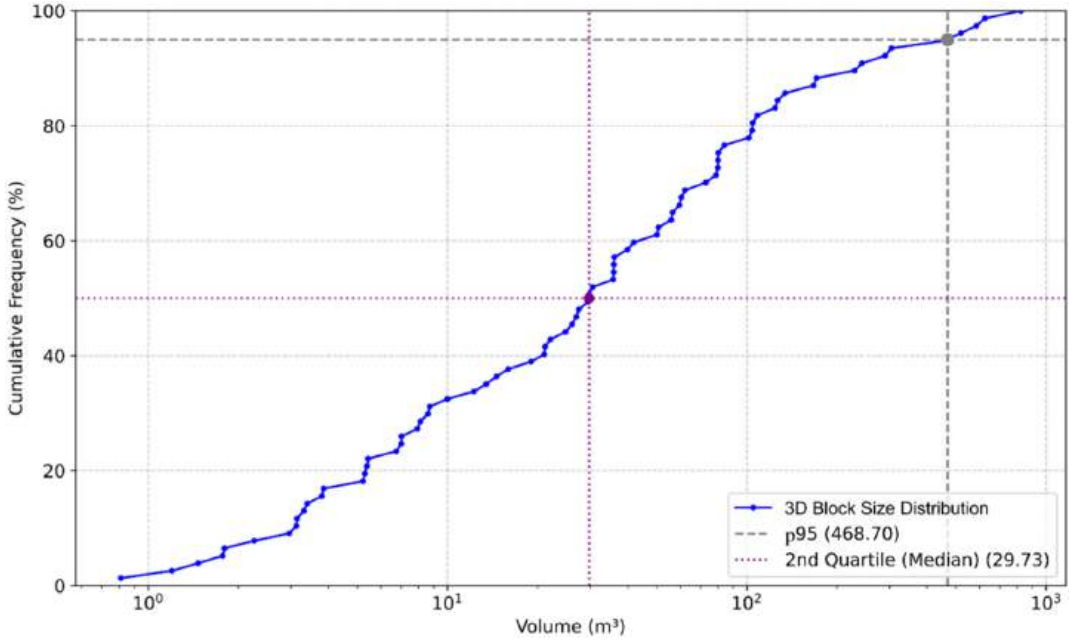

Figs. 10. 3D Block Size Distribution for the dataset of volumes analyzed for a portion of the slope of Mount Gallo. The 95th percentile and median values are highlighted. Modified from ABLOMOV results.

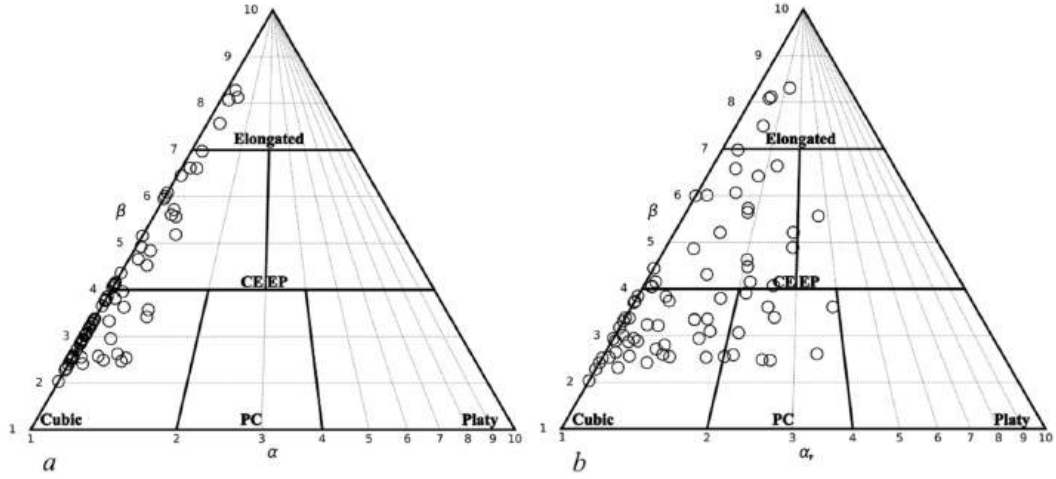

Fig. 11. Shape classification for the potentially unstable block dataset according to Kalenchuk shape classification (a) and β-α_F shape classification (b). CE (Cubic-Elongated), EP (Elongated-Platy), and PC (Platy-Cubic) are the intermediate shapes between Cubic (C), Elongated (E), and Platy (P). Modified from ABLOMOV results.

photogrammetry processing for rock mechanics purposes. Convex Hull (CH) algorithm was then applied to the point clouds for the creation of new meshes and the calculation of volume and area (Fig. 14).

From the results in Fig. 14, a variation in area calculation of 0.13% for the cube, 0.02% for the sphere, and 0.03% for the cylinder can be observed when comparing the lowest and highest resolutions. The volume calculation is not affected by the lower resolution for the cube and is affected in a completely negligible way for the sphere and cylinder.

Moreover, a sensitivity analysis aimed at analyzing the influence of completeness of input data was performed on a cube 1m-length based on the completeness conditions defined in the Methodology section. The modified point clouds were modelled with the Convex Hull algorithm to obtain the meshes, and the results are summarized in Fig. 15.

What is observed is that in the area calculation, there is a variation of 0.03% in the case a, 0.5% in the case b, 0.6% in the case c, and 27.3% in the case d. In the volume calculation, there is a variation of 0.01% in the case a, 0.05% in the case b, 0.08% in the case c, and 50.8% in the case d.

Moreover, this approach was applied to a block of the entire 77-blocks dataset. On the block, which has three outcropping faces (F1, F2, F3 in fig., 16), the meshing algorithm was applied by varying the resolution of the starting point cloud (0.5 cm, 1 cm, and 2 cm). The calculated volumes and surface areas deviate respectively by 0.32% and 0.22% when going from a lower to a higher resolution (Fig., 16a).

The influence of the completeness of the input data on the definition of the block size was carried out according to three cases, excluding one of the three faces each time. Considering a reference resolution *s* equal to 1 cm, the real volume and surface area were defined as 6.881 m^3 and 21.590 m^2, respectively. The results obtained highlight a greater proximity to the true values when face F3 is included in the calculation (Fig. 16b). In fact, the block with F1-F3 faces deviates by 17.12% for the volume and 11.5% for the surface, while the block with F2-F3 faces deviates by 21.8% for the volume and 10.1% for the surface. In the case

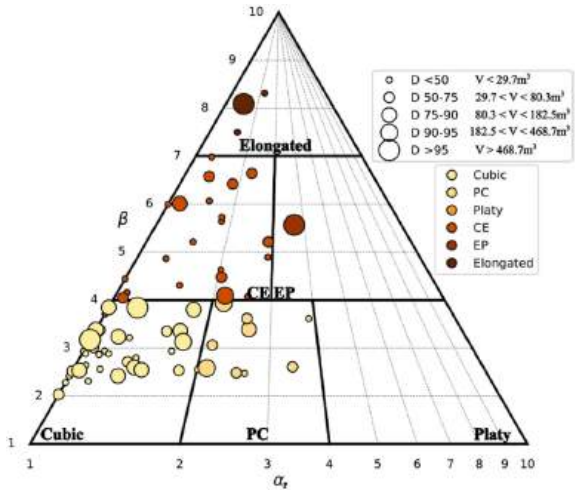

Fig. 12. Classification of shapes with volumetric information divided into size classes from 3D Block Size Distribution according to β-αF classification system. CE, EP, and PC are the intermediate shapes between Cubic, Elongated, and Platy. Modified from ABLOMOV results.

where the absence of face F3 is simulated, there is a discrepancy of 49.3% for the volume and 31% for the surface.

4.3. Uncertainty analysis

Sample size sufficiency was assessed through a convergence analysis by comparing the 95th percentile (p95) and its corresponding 95% Confidence Interval (CI) across randomized data subsets. The full results are provided in the Supplementary Material, Note C.

The uncertainty analysis conducted in two phases according to the proposed nested approach was applied to the volumetric dataset presented for case study 2. The outputs are the 95% confidence interval with respect to the 3D-BSD (Fig. 17) and the calculation of the coverage and inclusion rates.

Starting from the 3D-BSD, the 95th percentile (95p) was defined as the reference statistic and is equal to 471.84 m^3. The confidence interval constructed according to the Outer Bootstrap process defined, with a 95% probability, that the 95th percentile falls within an interval between 229.11 and 674.52 m^3.

The Inner Bootstrap process defined a coverage rate of 94.7% and an inclusion rate of 88.5%.

5. Discussion

This work introduces a robust and innovative method for characterizing potentially unstable rock blocks using high-resolution 3D point clouds. The process involves block segmentation (via CloudCompare) and the creation of watertight 3D models using the Convex Hull algorithm, ensuring realistic volume and surface determination. The core of the methodology lies in integrating 3D Block Size Distribution analysis with a modified block shape classification system. As demonstrated by tests on primitive (Fig. 7, Table 1) and real shapes (Figs. 8 and 11), the introduction of a correction coefficient *F* derived from OMBB dimensions, optimizes the flattening index, thereby enhancing the accuracy of the shape classification system. This comprehensive approach provides quantitative parameters essential for rockfall risk assessment and mitigation. The method was validated on synthetic dataset and successfully applied to 77 real blocks from Mount Gallo, Sicily.

The results obtained from the real case study show that smaller and intermediate rock classes predominantly exhibit a cubic shape. However, larger rock classes exhibit a more heterogeneous behavior, with a tendency toward a platy and elongated shapes.

In this regard, Watman et al.,[20] demonstrated how rock mass structure and kinematic feasibility dictate rockfall shape and size distribution by comparing DFN derived BSD and change detection derived BSD.

Kalenchuk et al. (2006) suggested that large blocks can exhibit different shapes compared to smaller ones. Their reasoning was that the average orientation of joint sets dictates the primary shape of the rock mass, which they also concluded would represent the largest size fraction. The results of the present work align with these conclusions with some exceptions. In particular, the fact that two of the four blocks in the largest dimensional class are among those that deviate from the general trend is a critical factor that highlights the effectiveness of the proposed method. In fact, by applying traditional approaches for defining the characteristic volume based on the main discontinuity sets, there would be an underestimation of the larger percentiles as they are partly determined by blocks isolated by statistically rare discontinuities.

The sensitivity analysis confirmed the robustness of the volume calculation method with respect to the resolution of the input data, with

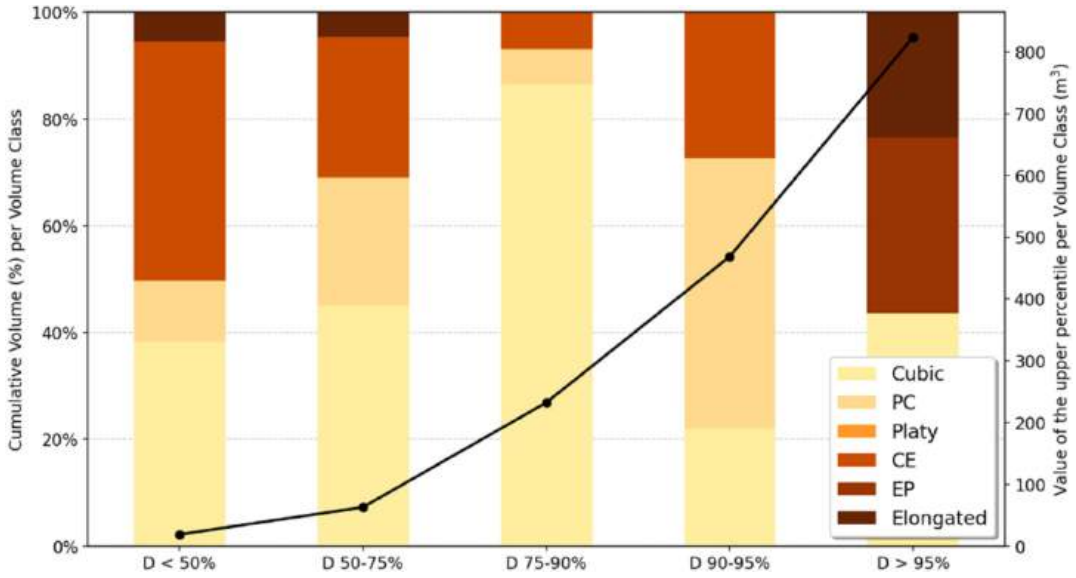

Fig. 13. Stacked Bar Chart representing the relative frequency of shapes for each size class. The volumetric values (m^3) corresponding to the upper percentiles for each class are also represented.

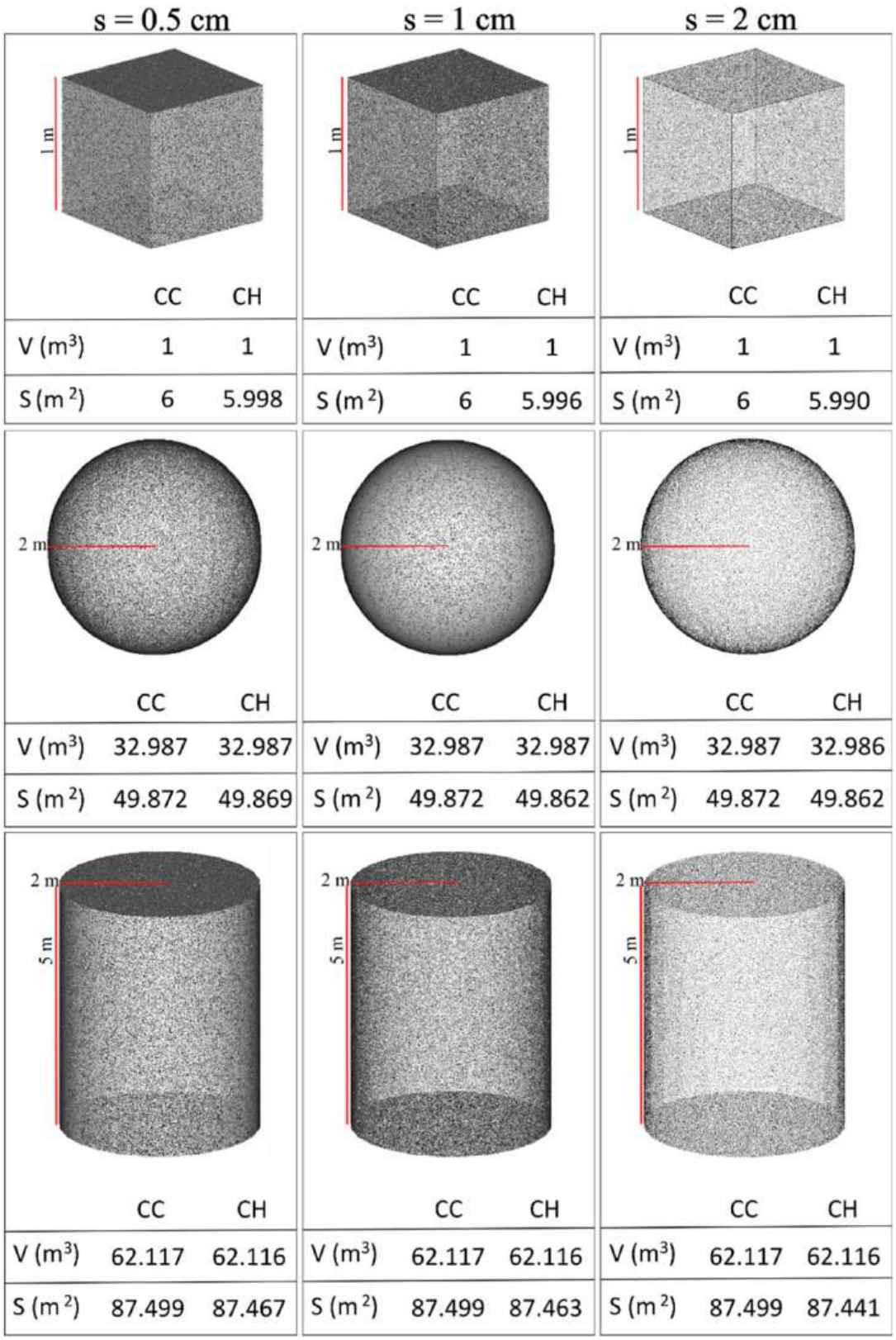

Fig. 14. Comparison of volume and surface area calculated on CloudCompare (CC) and applying the algorithm of Convex Hull (CH) for cube, sphere, cylinder for different resolution of the point clouds.

negligible variations as the quality of the starting data decreased.

Specifically, an aspect that emerges from the input-data resolution test is that the volumes of solids generated from 3D point clouds, such as a cube, show a slight difference in sensitivity to resolution variations compared to the surface areas. Indeed, since volume is a global measure, it tends to remain stable even in the presence of low-density point clouds. A point cloud that approximates a 1 m side cube generates a Convex Hull with a volume that approximates 1 m^3, regardless of the

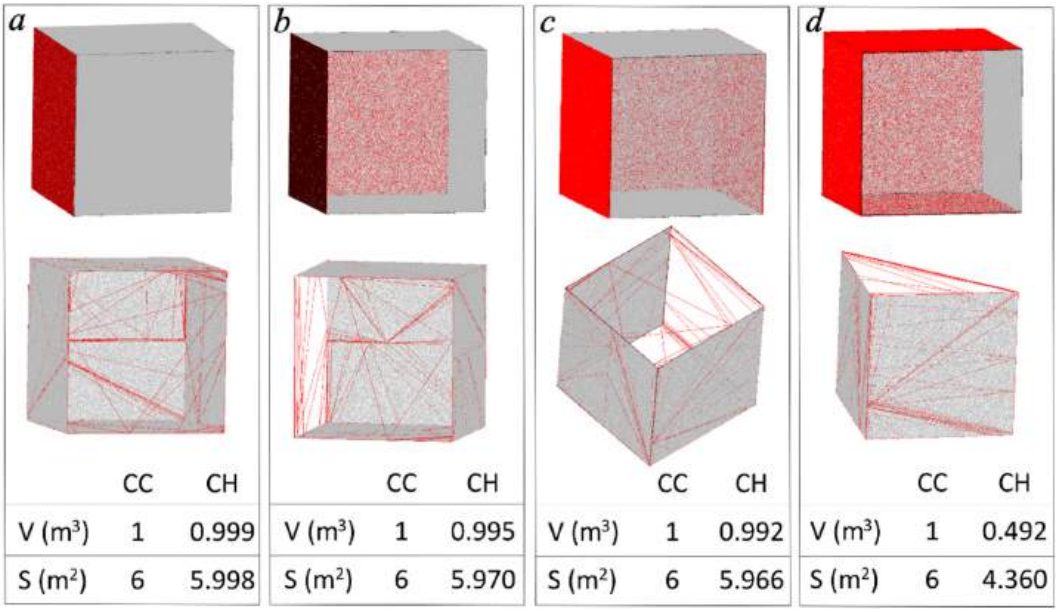

	CC	CH
V (m³)	1	0.999
S (m²)	6	5.998

	CC	CH
V (m³)	1	0.995
S (m²)	6	5.970

	CC	CH
V (m³)	1	0.992
S (m²)	6	5.966

	CC	CH
V (m³)	1	0.492
S (m²)	6	4.360

Fig. 15. Calculation of volume and surface area by applying the Convex Hull algorithm (CH), as the completeness of the point cloud varies compared to the original volume and surface area (CC). Convex Hull models resulting from ABLOMOV tool.

data precision. The surface area, conversely, is a much more local measure that is sensitive to imperfections. With a low resolution, the created mesh coarsely approximates the surface, resulting in a calculated area smaller than the theoretical 6 m^2. As the resolution increases, the mesh adapts better to the real shape, and the calculated surface area progressively approaches the correct value.

However, data completeness showed a significant impact, especially in cases where the faces essential for defining the real volume and surface are absent or poorly represented (e.g., a cubic block where only two faces are exposed). Specifically, the reliability of volume estimation decreases when the degree of protrusion (i.e., the exposed surface area) falls under 50%. This highlights the main limitation in the characterization of potentially unstable blocks by using point clouds, as already concluded by Chen et al.[52] This issue can be mitigated for regular-shaped blocks by applying the geometric correction factors suggested by Wang et al.[53] for low-protrusion blocks.

Since the Convex Hull algorithm generates the smallest convex set containing the point cloud, it inherently bridges surface concavities and closes the hidden back face by connecting the vertices of the segmentation boundary. Consequently, the calculated volume represents a theoretical upper bound.

While DiFrancesco et al.[54] demonstrate the tendency of the convex hull algorithm to overestimate, they further observe that the results converge with those proposed by the same authors (i.e., Alpha Solid method), so long as the blocks do not exhibit pronounced concavities. This corresponds to the characteristics of the blocks in this study. Furthermore, the advantages of the Convex Hull algorithm for defining blocks with occluded back surfaces, as highlighted by Wang et al.,[53] is equally applicable to our approach. Therefore, regarding the hidden rear surface, the algorithm does not assume a strictly planar cut but rather generates a closing surface that maintains convexity based on the block's perimeter.

Moreover, the same authors observed strong consistency when comparing their automated segmentation method (based on the Segment Anything Model) with the manual, expert-guided segmentation proposed by Mineo et al.,[14] which is the methodology adopted in this work.

Given that ABLOMOV is intended for expert users, careful application is required to mitigate the risks of volume overestimation or, more critically, underestimation.

Currently, the main limitation is the time required to manually identify and segment the blocks. However, as ABLOMOV requires previously segmented blocks to conduct size and shape analysis, the workflow allows for the integration of diverse segmentation techniques in the pre-processing phase, such as those leveraging Large Language Models.[53,55]

In contrast to multi-temporal analyses, the proposed method focuses on potentially unstable blocks, thereby eliminating dependencies on monitoring frequency choices[18] and multi-temporal point cloud resolution.[19,56] However, adopting a comparative framework similar to Watman et al.[20] to cross-reference the proposed 3D-BSD with change detection data would significantly improve the understanding of structural controls within the studied rock mass also allowing defining which blocks are actually unstable among the recognized potential ones. Uncertainty analysis, conducted with a non-parametric approach based on nested BCA Bootstrap, provided a robust estimate of the reliability of the statistics derived from the 3D Block Size Distribution. The coverage rate (94.7%) and inclusion rate (88.5%) values indicate that the 95% confidence interval constructed is a good estimator of uncertainty, and that the sample dataset is a consistent and stable representation of the population, supporting the inferential repeatability of the results (see supplementary material, note C). This approach is particularly suitable for quantifying the uncertainties on volumetric datasets of small size and with high dispersion,[57] typically resulting from remote analysis for rock masses.

6. Conclusions

The method developed in this study offers a robust and quantitative approach for the characterization of potentially unstable blocks starting from high-resolution point clouds. The combination of segmentation techniques, 3D modelling based on Convex Hull, statistical analysis of dimensional distribution, and a refined morphometric classification, allows obtaining information useful to produce a high-fidelity simulation of rockfall propagation, overcoming some limitations of simplified propagation models.

To simplify the application of the proposed method, the Advanced BLOck MOrphometry and Volume analyser (ABLOMOV) was developed in Python environment. Point clouds representing the blocks can be loaded as input in the most common formats (.txt, .obj, .las). The first

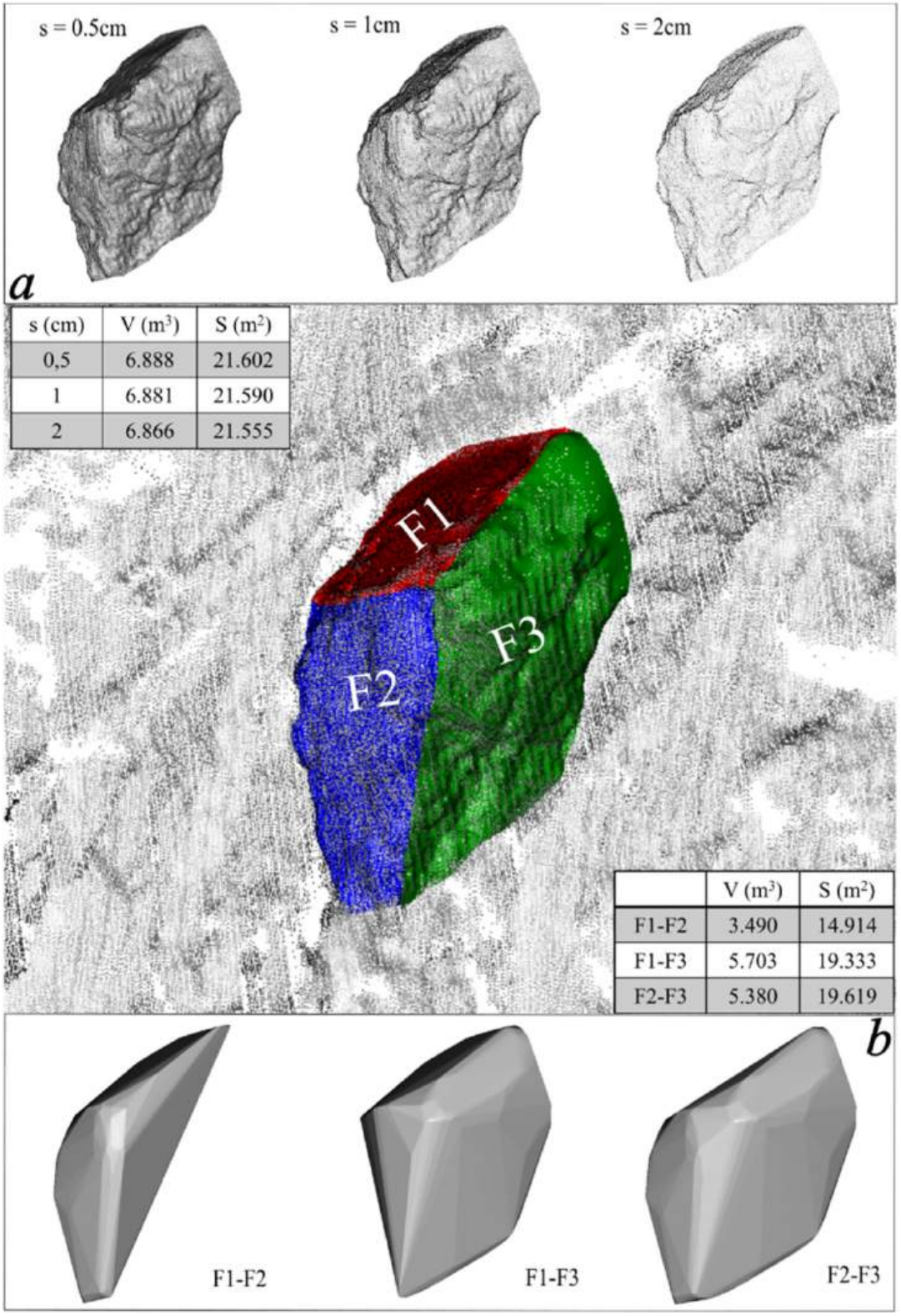

Fig. 16. Sensitivity analysis applied on a real block a) by varying resolution as spacing between points. b) by varying the completeness of the studied object. Convex Hull models resulting from ABLOMOV tool.

calculation step involves defining the Convex Hull model for each block, from which its volume (m^3) and surface area (m^2) can be calculated.

Functions to perform, visualize and export the 3D Block Size Distribution were implemented as well as the possibility to export the volume and surface area information for each point cloud in. xlsx format. Moreover, the modelled blocks can be exported as 3D meshes in. obj format.

The tool allows for calculation of morphometric parameters (α_F, β) and plotting on the triangular diagram for shape classification purposes. Once the volumetric classes are defined based on 3D-BSD, they can be

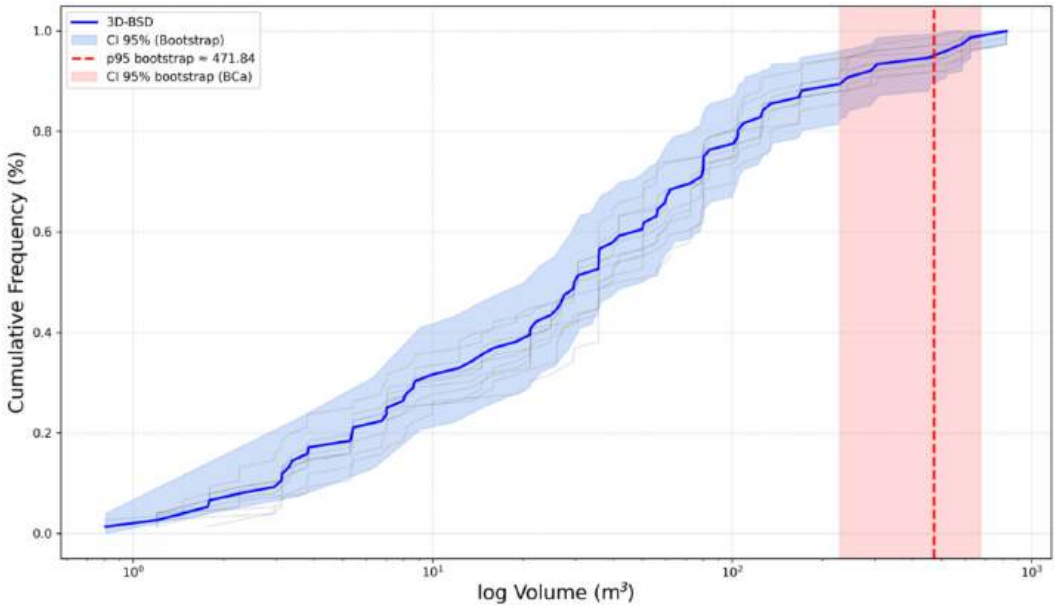

Fig. 17. Graphical representation of the 3D-BSD (blue) with its 95% confidence interval (light blue) constructed with BCA Bootstrap. The 95p (red dashed line) of 471.84 m^3 and the corresponding 95% CI, ranging between 229.11 and 674.52 m^3, are highlighted. Modified from ABLOMOV results.

integrated into the shape triangular diagram and exported. An outstanding issue is the choice of statistics for design purposes, particularly on the selection between the highest percentile (90–95th) and the upper confidence limit at 95%.

Future developments of this work will aim to validate the proposed method by comparing the identified potentially unstable blocks with actual rockfall occurrences detected through long-term monitoring, adopting a comparative framework.

CRediT authorship contribution statement

G. Mineo: Writing – review & editing, Writing – original draft, Visualization, Validation, Software, Methodology, Investigation, Formal analysis, Data curation, Conceptualization. **A. Riquelme:** Writing – review & editing, Visualization, Validation, Supervision, Methodology, Conceptualization. **M. Rosone:** Writing – review & editing, Writing – original draft, Visualization, Validation, Supervision, Methodology, Formal analysis, Data curation, Conceptualization. **C. Cappadonia:** Writing – review & editing, Writing – original draft, Visualization, Validation, Supervision, Methodology, Formal analysis, Data curation, Conceptualization.

Declaration of competing interest

The authors declare that they have no known competing financial interests or personal relationships that could have appeared to influence the work reported in this paper.

Appendix A. Supplementary data

Supplementary data to this article can be found online at https://doi.org/10.1016/j.ijrmms.2026.106477.

Data availability

Code and GUI available at: https://github.com/giampiero-mineo/ABLOMOV-Advanced-BLOck-MOrfometric-and-Volume-analyser-.git (github).

References

1. Mauldon M. Intersection probabilities of impersistent joints. *Int J Rock Mech Min Sci Geomech Abstracts*. 1994;31(2):107–115. https://doi.org/10.1016/0148-9062(94)92800-2.
2. ISRM. Suggested methods for determining tensile strength of rock materials. *Int J Rock Mech Min Sci Geomech Abstracts*. 1978;15(3):99–103. https://doi.org/10.1016/0148-9062(78)90003-7.
3. Abellan A, Derron MH, Jaboyedoff M. "Use of 3D Point Clouds in Geohazards" special issue: current challenges and future trends. *Remote Sens*. 2016;8(2):130. https://doi.org/10.3390/rs8020130.
4. Chen JL, Bo LH, Jiang N, Chen Q, Yang YC, Zhou JW. Stability evaluation of shallow blocks in high and steep slope combining TLS and UAV photogrammetry. *Geomat Nat Hazards Risk*. 2025;16(1), 2464052. https://doi.org/10.1080/19475705.2025.2464052.
5. Gigli G, Lombardi L, Carlà T, Beni T, Casagli N. A method for full three-dimensional kinematic analysis of steep rock walls based on high-resolution point cloud data. *Int J Rock Mech Min Sci*. 2022;157, 105178. https://doi.org/10.1016/j.ijrmms.2022.105178.
6. Cappadonia C, Cafiso F, Ferraro R, Martinello C, Rotigliano E. Analysis of the rockfall phenomena contributing to the evolution of a pocket beach area using traditional and remotely acquired data (Lo Zingaro nature reserve, Southern Italy). *Remote Sens*. 2023;15(5):1401. https://doi.org/10.3390/rs15051401.
7. Jordá Bordehore L, Riquelme A, Cano M, Tomás R. Comparing manual and remote sensing field discontinuity collection used in kinematic stability assessment of failed rock slopes. *Int J Rock Mech Min Sci*. 2017;97:24–32. https://doi.org/10.1016/j.ijrmms.2017.06.004.
8. Mineo G, Rosone M, Cappadonia C. Hazard assessment of a rocky slope of Mount pellegrino (northern sicily): a comparative study of direct and indirect approaches. *Italian J Eng Geol Environ*. 2024;1(2024_1S):205. https://doi.org/10.4408/IJEGE.2024-01.S-23.
9. Sarro R, Riquelme A, García-Davalillo J, et al. Rockfall simulation based on UAV photogrammetry data obtained during an emergency declaration: application at a cultural heritage site. *Remote Sens*. 2018;10(12):1923. https://doi.org/10.3390/rs10121923.
10. Dewez TJB, Girardeau-Montaut D, Allanic C, Rohmer J. Facets : a cloudcompare plugin to extract geological planes from unstructured 3D point clouds. *Int Arch Photogram Rem Sens Spatial Inf Sci*. 2016;XLI-B5:799–804. https://doi.org/10.5194/isprsarchives-XLI-B5-799-2016.
11. Riquelme AJ, Abellán A, Tomás R, Jaboyedoff M. A new approach for semi-automatic rock mass joints recognition from 3D point clouds. *Comput Geosci*. 2014;68:38–52. https://doi.org/10.1016/j.cageo.2014.03.014.
12. Caliò D, Mineo S, Pappalardo G. Digital rock mass analysis for the evaluation of rockfall magnitude at poorly accessible cliffs. *Remote Sens*. 2023;15(6):1515. https://doi.org/10.3390/rs15061515.
13. Mastrantoni G, Santicchia G, Cosentino A, Molinari A, Marmoni GM, Mazzanti P. Automatic photomonitoring analysis for spatiotemporal evaluation of rockfall failure hazard. *Eng Geol*. 2024;339, 107662. https://doi.org/10.1016/j.enggeo.2024.107662.
14. Mineo G, Rosone M, Cappadonia C. Semi-automated rock block volume extraction from high-resolution 3D point clouds for enhanced rockfall hazard analysis. *Int J*

Rock Mech Min Sci. 2025;185, 105982. https://doi.org/10.1016/j.ijrmms.2024.105982.
15. Farmakis I, Guccione DE, Thoeni K, Giacomini A. VoxFall: Non-parametric volumetric change detection for rockfalls. *Eng Geol*. 2025;352, 108045. https://doi.org/10.1016/j.enggeo.2025.108045.
16. Carrea D, Abellan A, Derron MH, Jaboyedoff M. Automatic rockfalls volume estimation based on terrestrial laser scanning data. In: Lollino G, Giordan D, Crosta GB, et al., eds. *Engineering Geology for Society and Territory - Volume 2*. Springer International Publishing; 2015:425–428. https://doi.org/10.1007/978-3-319-09057-3_68.
17. DiFrancesco PM, Bonneau D, Hutchinson DJ. The implications of M3C2 projection diameter on 3D semi-automated rockfall extraction from sequential terrestrial laser scanning point clouds. *Remote Sens*. 2020;12(11):1885. https://doi.org/10.3390/rs12111885.
18. Williams JG, Rosser NJ, Hardy RJ, Brain MJ. The importance of monitoring interval for rockfall magnitude-frequency estimation. *JGR Earth Surface*. 2019;124(12):2841–2853. https://doi.org/10.1029/2019JF005225.
19. Guerin A, Stock GM, Radue MJ, et al. Quantifying 40 years of rockfall activity in Yosemite valley with historical structure-from-motion photogrammetry and terrestrial laser scanning. *Geomorphology*. 2020;356, 107069. https://doi.org/10.1016/j.geomorph.2020.107069.
20. Watman A, Guccione DE, Thoeni K, Giacomini A. From rock mass to rockfall activity: a comprehensive rockfall assessment using 3D kinematic analysis and change detection. *Eng Geol*. 2025;359, 108437. https://doi.org/10.1016/j.enggeo.2025.108437.
21. Palmstrøm A. Characterizing rock masses by the RMi for use in practical rock engineering. *Tunn Undergr Space Technol*. 1996;11(2):175–188. https://doi.org/10.1016/0886-7798(96)00015-6.
22. Lu P, Latham JP. Developments in the assessment of In-situ block size distributions of rock masses. *Rock Mech Rock Eng*. 1999;32(1):29–49. https://doi.org/10.1007/s006030050042.
23. Wang H, Latham JP, Poole AB. Predictions of block size distribution for quarrying. *QJEGH*. 1991;24(1):91–99. https://doi.org/10.1144/GSL.QJEG.1991.024.01.10.
24. Umili G, Bonetto SMR, Mosca P, Vagnon F, Ferrero AM. In situ block size distribution aimed at the choice of the design block for rockfall barriers design: a case study along gardesana road. *Geosciences*. 2020;10(6):223. https://doi.org/10.3390/geosciences10060223.
25. Caviezel A, Ringenbach A, Demmel SE, et al. The relevance of rock shape over mass—implications for rockfall hazard assessments. *Nat Commun*. 2021;12(1):5546. https://doi.org/10.1038/s41467-021-25794-y.
26. Zingg. Beitrag zur schotteranalyse. Published online https://www.research-collection.ethz.ch/bitstream/handle/20.500.11850/135183/eth-21472-01.pdf; 1935.
27. Sneed ED, Folk RL. Pebbles in the lower Colorado river, Texas a study in particle morphogenesis. *J Geol*. 1958;66(2):114–150. https://doi.org/10.1086/626490.
28. Palmström A, Singh R. The deformation modulus of rock masses — comparisons between in situ tests and indirect estimates. *Tunn Undergr Space Technol*. 2001;16(2):115–131. https://doi.org/10.1016/S0886-7798(01)00038-4.
29. Wang LG, Yamashita S, Sugimoto F, Pan C, Tan G. A methodology for predicting the in situ size and shape distribution of rock blocks. *Rock Mech Rock Eng*. 2003;36(2):121–142. https://doi.org/10.1007/s00603-002-0039-8.
30. Smith JV. Determining the size and shape of blocks from linear sampling for geotechnical rock mass classification and assessment. *J Struct Geol*. 2004;26(6-7):1317–1339. https://doi.org/10.1016/j.jsg.2003.11.019.
31. Kalenchuk KS, Diederichs MS, McKinnon S. Characterizing block geometry in jointed rockmasses. *Int J Rock Mech Min Sci*. 2006;43(8):1212–1225. https://doi.org/10.1016/j.ijrmms.2006.04.004.
32. Kong D, Saroglou C, Wu F, Sha P, Li B. Development and application of UAV-SfM photogrammetry for quantitative characterization of rock mass discontinuities. *Int J Rock Mech Min Sci*. 2021;141, 104729. https://doi.org/10.1016/j.ijrmms.2021.104729.
33. Mahdavirad M, Saeidi A, Shahbazi A, Noël JF. Development of a novel equation for estimating the average volume of rock blocks in a rock mass with non-persistent joints. *Bull Eng Geol Environ*. 2025;84(1):14. https://doi.org/10.1007/s10064-024-03992-4.
34. Rasmussen LL. U n B l o c k s g e n : a Python library for 3D rock mass generation and analysis. *SoftwareX*. 2020;12, 100577. https://doi.org/10.1016/j.softx.2020.100577.
35. Yan J, Chen J, Zhang Y, et al. Semi-automatic extraction of dangerous rock blocks from jointed rock exposures based on a discontinuity trace map. *Comput Geotech*. 2023;156, 105265. https://doi.org/10.1016/j.compgeo.2023.105265.
36. Zhou Y, Fu H, Zhou M, Zhao Y, Chen J. A new framework for automated extraction of in-situ dangerous rock blocks based on a semi-deterministic block theory. *Bull Eng Geol Environ*. 2025;84(3):119. https://doi.org/10.1007/s10064-025-04107-3.
37. Bonneau D, DiFrancesco PM, Hutchinson DJ. Surface reconstruction for three-dimensional rockfall volumetric analysis. *IJGI*. 2019;8(12):548. https://doi.org/10.3390/ijgi8120548.
38. Wang H, Latham JP, Poole AB. Predictions of block size distribution for quarrying. *QJEGH*. 1991;24(1):91–99. https://doi.org/10.1144/GSL.QJEG.1991.024.01.10.
39. ONR 24810; Austrian Standards Institute. *Technical Protection Against Rockfall—Terms and Definitions, Effects of Actions, Design, Monitoring and Maintenance*. 2017. Published online.
40. UNI 11211-3. *Opere Di Difesa Dalla Caduta Massi - Parte 3: Progetto Preliminare*. 2018. Published online 2018.
41. Anderson TW, Darling DA. Asymptotic theory of certain "Goodness of Fit" criteria based on stochastic processes. *Ann Math Statist*. 1952;23(2):193–212. https://doi.org/10.1214/aoms/1177729437.
42. Massey FJ. The kolmogorov-smirnov test for goodness of fit. *J Am Stat Assoc*. 1951;46(253):68–78. https://doi.org/10.1080/01621459.1951.10500769.
43. Shapiro SS, Wilk MB. An analysis of variance test for normality (complete samples). *Biometrika*. 1965;52(3-4):591–611. https://doi.org/10.1093/biomet/52.3-4.591.
44. Carriero MT, Ferrero AM, Migliazza MR, Umili G. Effect of uncertainties on block volume estimation. *IOP Conf Ser Earth Environ Sci*. 2023;1124(1), 012005. https://doi.org/10.1088/1755-1315/1124/1/012005.
45. Umili G, Taboni B, Ferrero AM. Influence of uncertainties: a focus on block volume and shape assessment for rockfall analysis. *J Rock Mech Geotech Eng*. 2023;15(9):2250–2263. https://doi.org/10.1016/j.jrmge.2023.03.016.
46. DiCiccio TJ, Efron B. Bootstrap confidence intervals. *Stat Sci*. 1996;11(3). https://doi.org/10.1214/ss/1032280214.
47. Lo Medico F, Varrica D, Zuccolini MV, Miola M, Scopelliti G, Alaimo MG. Geochemical baseline values and spatial distribution of major, trace, and rare earth elements in unpolluted soils of the Sicily region (Italy). *Environ Geochem Health*. 2025;47(5):167. https://doi.org/10.1007/s10653-025-02475-z.
48. Manly BFJ. *Randomization, Bootstrap and Monte Carlo Methods in Biology*. 0 ed. Chapman and Hall/CRC; 2018. https://doi.org/10.1201/9781315273075.
49. Soltis PS, Soltis DE. Applying the bootstrap in phylogeny reconstruction. *Stat Sci*. 2003;18(2). https://doi.org/10.1214/ss/1063994980.
50. Varrica D, Lo Medico F, Zuccolini MV, Miola M, Alaimo MG. Geochemical baseline values determination and spatial distribution of trace elements in topsoils: an application in sicily region (Italy). *Sci Total Environ*. 2024;955, 176951. https://doi.org/10.1016/j.scitotenv.2024.176951.
51. Cafiso F, Cappadonia C, Ferraro R, Martinello C. Rockfall hazard assessment of the Monte Gallo oriented nature reserve area (southern Italy). *IOP Conf Ser Earth Environ Sci*. 2021;833(1), 012176. https://doi.org/10.1088/1755-1315/833/1/012176.
52. Chen N, Kemeny J, Jiang Q, Pan Z. Automatic extraction of blocks from 3D point clouds of fractured rock. *Comput Geosci*. 2017;109:149–161. https://doi.org/10.1016/j.cageo.2017.08.013.
53. Wang J, Zheng J, Hu J, et al. In-situ block intelligent identification: large-scale artificial intelligence (AI) models enable efficient geological surveys via image segmentation. *Eng Geol*. 2025;356, 108286. https://doi.org/10.1016/j.enggeo.2025.108286.
54. DiFrancesco PM, Bonneau DA, Hutchinson DJ. Computational geometry-based surface reconstruction for volume estimation: a case study on magnitude-frequency relations for a LiDAR-Derived rockfall inventory. *IJGI*. 2021;10(3):157. https://doi.org/10.3390/ijgi10030157.
55. Wang J, Zheng J, Hu J, et al. An interactive framework integrating segment anything model and structure-from-motion for three-dimensional discontinuity identification in rock masses. *Int J Min Sci Technol*. 2025;35(10):1695–1711. https://doi.org/10.1016/j.ijmst.2025.09.005.
56. Kromer RA, Hutchinson DJ, Lato MJ, Gauthier D, Edwards T. Identifying rock slope failure precursors using LiDAR for transportation corridor hazard management. *Eng Geol*. 2015;195:93–103. https://doi.org/10.1016/j.enggeo.2015.05.012.
57. Hesterberg TC. What teachers should know about the bootstrap: resampling in the undergraduate statistics curriculum. *Am Statistician*. 2015;69(4):371–386. https://doi.org/10.1080/00031305.2015.1089789.